

Alternative method for measuring characteristic lengths in absorbing phase transitionsJin Min Kim^{✉*} and Sang Bub Lee^{✉†}*Department of Physics and OMEG Institute, Soongsil University, Seoul 06978, Korea* (Received 13 August 2021; accepted 26 January 2022; published 9 February 2022)

We applied an alternative method for measuring characteristic lengths reported recently by one of us [J. M. Kim, *J. Stat. Mech.* (2021) 033213] to the models in the Manna universality class, i.e., the stochastic Manna sandpile and conserved lattice gas models in various dimensions. The universality of the Manna model has been under long debate particularly in one dimension since the work of M. Basu *et al.* [*Phys. Rev. Lett.* **109**, 015702 (2012)], who claimed that the Manna model belongs to the directed percolation (DP) universality class and that the independent Manna universality class does not exist. We carried out Monte Carlo simulations for the stochastic Manna sandpile model in one, two, and three dimensions and the conserved lattice gas model in three dimensions, using both the natural initial states (NISs) and uniform initial states (UISs). In two and three dimensions, the results for $R(t)$, defined by $R(t) = L[\langle \rho_a^2 \rangle / \langle \rho_a \rangle^2 - 1]^{1/d}$, L and ρ_a being, respectively, the system size and activity density, yielded consistent results for the two initial states. $R(t)$ is proportional to the correlation length following $R(t) \sim t^{1/2}$ at the critical point. In one dimension, the data of $R(t)$ for the Manna model using NISs yielded anomalous behavior, suggesting that NISs require much longer prerun time steps to homogenize the distribution of particles and larger systems to eliminate the finite-size effect than those employed in the literature. On the other hand, data from UISs yielded a power-law behavior, and the estimated critical exponents differed from the values in the DP class.

DOI: [10.1103/PhysRevE.105.025307](https://doi.org/10.1103/PhysRevE.105.025307)**I. INTRODUCTION**

The purpose of this paper is to study the critical behavior of absorbing phase transitions (APTs) [1,2] for models in the Manna universality class or, often called, conserved directed percolation class [3], in dimensions below the critical dimension of $d_c = 4$, by applying an alternative method for measuring characteristic lengths [4] coupled with a conventional method. Several models such as various fixed-energy sandpile models [5–7], conserved threshold transfer processes [8,9], the conserved lattice gas (CLG) model [10–12], and static diffusive epidemic processes [13–15] have been known to share the same features of the critical behavior. For these models, it was conjectured that in the absence of additional symmetries the stochastic models with infinitely many absorbing states and activity coupled to a nondiffusive conserved field form a unique universality class [10].

Recently, Basu *et al.* [16] raised, based on numerical simulations in one dimension, the question of whether the Manna universality class is indeed an independent class or is simply a perturbation of the directed percolation (DP) class [17]. They paid attention to the fact that for models in the Manna class the estimates of critical exponents are scattered depending on the authors and show anomalous scaling relations. The decay of activity $\rho_a(t) \sim t^{-\theta}$ starting from many activities and of the survival probability of activity $P_s(t) \sim t^{-\delta}$ starting from a single seed are characterized by different exponents,

whereas the order-parameter exponents β for the two cases are consistent within errors [10,18]. Moreover the upper critical dimension $d_c = 4$ and the mean-field exponents in the Manna class are the same as those in the DP class. In addition, the corresponding models with self-organized criticality are known to be unstable against specific perturbation and generally flow to DP [19]. They conjectured that the non-DP behavior is also a transient phenomenon and all models with such behaviors eventually show a DP critical behavior after a very long time.

In most models in the APTs, the system evolves from a homogeneous distribution of particles. For example, for a prototype in the DP class, i.e., for the contact process (CP) [20], simulations have been carried out from the initial states very close to or far from the absorbing state. In the CP, each particle either creates an offspring on a neighboring site with a rate λ or annihilates with a rate μ ; if $\lambda > \lambda_c$, the system remains in an active phase and, if $\lambda < \lambda_c$, the system falls into an absorbing state of a vacuum. The system starts with either a fully occupied lattice system or a single-particle system. The former is called “static” simulation and the latter “dynamic” simulation, and in both cases, the initial state is unique. While in the CP the initial particle distribution is homogeneous and uniform, that in models with a conserved field (fixed number of particles) is not unique or homogeneous. The possible concern might be whether the initial distribution influences the critical behavior. Basu *et al.* realized such a possibility from the earlier work by Jensen and Dickman who studied the APTs of the pair-contact process [21]. In the pair-contact process, the system starting from a random initial distribution of particles exhibited considerably different dynamical behaviors from the system with particularly prepared initial states, i.e., system-generated initial states. For a system-generated

*jmkim@ssu.ac.kr

†Professor Emeritus, Kyungpook National University, Daegu 41566, Korea; sblee@knu.ac.kr

initial state, the simulation first ran on a smaller system over a number of time steps, and then a larger system was set up by combining copies of the smaller system. The particle distribution of such initial states is random on a smaller scale but is uniform on a larger scale. Earlier works for models in the Manna class employed random initial states (RISs), and the anomalous behavior such as violation of scaling relations was observed [7,10,18,22,23]. In addition, particularly in one dimension, the activity density in the supercritical region did not monotonically decrease; it reached a minimum and then slowly increased to a steady-state value for the particle density close to the critical density. The possible origin of the “undershooting” is slowly varying distributions of inactive background particles that exhibit long-range correlations.

In order to resolve such an anomalous behavior, Basu *et al.* prepared the “natural” initial states (NISs) as follows: first let the process run until the long-range correlations are sufficiently smoothed out, and then reactivate the system by allowing all particles to diffuse a single Monte Carlo (MC) sweep. The initial states prepared in this way are homogeneous and resolve the problem of undershooting and scaling anomaly, and in addition, the particle distribution is known to be hyperuniform [24–26], in contrast to the random distribution for RISs. The exponents associated with dynamics of systems obtained using the NISs indeed differed from those using the RISs and they were close to the DP values in one dimension [16]. Since the work of Ref. [16], the critical behavior of the lattice models in the Manna class has been extensively studied in one and two dimensions. In one dimension, due to the subtleties of preparation of initial states, the reported critical exponents were dispersed [16,27–29]. While some authors obtained static critical exponents indeed similar to those of the DP class and claimed the Manna model to belong to the DP universality class [28], there were other researchers who claimed, based on distinct responses to the quenched disorder, the model to belong to the independent class that is different from the DP class [27,30]. In two dimensions, the critical exponents also differed considerably [31,32].

In this study, we apply an alternative method for measuring the correlation lengths [4] to APTs. In APTs, researchers have calculated the critical exponents associated with the correlation lengths indirectly via the scaling relations and scaling analysis because direct measurement of the correlation lengths is highly nontrivial task. For models in the Manna universality class, however, it is widely known that anomalous critical behavior hampers the scaling analysis and, in addition, the known scaling relation is violated when the initial distribution of particles is not properly homogenized [7,10,16,18]. Therefore, the method employed in this work may serve as an alternative way of measuring the critical exponents associated with the correlation lengths. We study the critical behavior of the Manna model in one, two, and three dimensions and the CLG model in three dimensions, using the homogeneous initial states. We first discuss the critical behavior in two and three dimensions to validate our method. We then study the Manna model in one dimension, focusing on the cause of the scattered critical exponents. In Sec. II, dynamic rules and MC methods for the studied models are presented, and the critical behaviors of APTs are briefly described. In Sec. III, the results

are presented with relevant discussions, and conclusions are derived in Sec. IV.

II. MODELS AND CRITICAL BEHAVIORS

The APTs of lattice models have been studied for long and the simulation methods and critical behaviors are now widely known. We thus review very briefly the models and simulation methods.

A. Stochastic Manna sandpile model

The original Manna model was designed to study self-organized criticality (SOC) with stochastic hopping. In the original work of SOC by Bak, Tang, and Wiesenfeld (BTW) [33], sand grains are added one at a time on randomly selected sites in an initially flat substrate of a square lattice, and sites that attain four or more grains are considered to become active. As grains are added one by one, the height of the grain column at each site gradually increases and, at a certain moment, the system has a single active site when four grains accumulate on one site. The dynamics start by toppling grains from an active site into the four nearest-neighbor sites, distributing one grain to each neighboring site. Neighboring sites may then become active as they receive grains from the toppling process. As the system evolves, a burst of toppling activities, called an avalanche, occurs. The avalanche terminates when all sites become inactive, at which point a new grain is added. In this process, the toppling is deterministic and grains on the boundary sites flow out of the system and dissipate. A few years later, a stochastic Manna sandpile model (MSM) was designed to study whether the stochastic toppling alters the dynamics of SOC [34]. In [34], a two-state version of the MSM was studied, in which no more than one particle is allowed to be at a site in the stationary state. When a new particle is added on the already occupied site, a hard core interaction throws all particles out from that site and particles are redistributed in a random manner among its neighbors. Cascades are created when some of the neighbors were already occupied and continued until no occupancy higher than one is present. It is known that the BTW model is Abelian; i.e., interchanging the toppling sequence from the same initial configuration leads to the same final configuration, whereas the MSM is non-Abelian. The two models are known to exhibit distinct critical behaviors.

The MSM has been modified to study the APT critical behavior in a way that initially a number of particles of density ρ are distributed at random over a given system with multiple occupancy allowed, and the sites with two or more particles are assumed to be active sites and empty or singly occupied sites are inactive sites. All particles on active sites topple to randomly selected nearest-neighbor sites. When particles on the boundary sites are to be dissipated, they are assumed to reenter the system from opposite sides by periodic boundary conditions, thus keeping the number of particles constant [5]. Starting from the initial states prepared as described in the subsequent subsection, an active site is selected at random from the list. Particles on the active site hop to randomly selected nearest-neighbor sites, with an increment of evolution time $t \rightarrow t + \frac{1}{N_a(t)}$, $N_a(t)$ being the number of active sites

at time t . The mean and mean-squared activity densities are saved whenever the evolution time first exceeds an integer within a bin of width $\Delta(\log_{10} t) = 0.02$. This allows us to save disk space and place the data of $\rho(t_k)$ evenly on a common-logarithmic scale of Monte Carlo time steps, where t_k is the sampled (smallest integer) time step in the k th bin.

For a given density of particles ρ , the density of active sites $\rho_a(t)$ will decrease rapidly in time if $\rho < \rho_c$, ρ_c being the critical particle density, and saturate to a steady-state density ρ_{sat} if $\rho > \rho_c$. Thus, ρ serves as a control parameter, and $\rho_a(t)$ and ρ_{sat} are, respectively, the activity and order parameter. At ρ_c , $\rho_a(t)$ decreases in time following the power law $\rho_a(t) \sim t^{-\theta}$, and for $\rho > \rho_c$, $\rho_{\text{sat}}(\Delta)$ follows $\rho_{\text{sat}} \sim \Delta^\beta$, where $\Delta \equiv \rho - \rho_c$ is the distance from criticality and θ and β are, respectively, the decay and order-parameter exponents. The temporal and spatial correlation lengths τ and ξ also exhibit power-law behaviors, $\tau \sim \Delta^{-\nu_{\parallel}}$ and $\xi \sim \Delta^{-\nu_{\perp}}$, where ν_{\parallel} (ν_{\perp}) is the temporal (spatial) correlation-length exponent. The critical exponents characterizing power laws of the survival probability $P_s(t) \sim t^{-\delta}$, number of active sites (particles) $N_s(t) \sim t^\eta$, and spreading distance of active sites $R_s(t) \sim t^{1/z}$ can also be calculated from dynamic simulations. Either the gyration ratio or the largest spanning distance of activity along any coordinate direction are considered to be the spreading distance. These critical exponents are not independent and are associated with each other via the scaling relations, $\nu_{\parallel} = \beta/\theta$, $z = \nu_{\parallel}/\nu_{\perp}$, and $d/z = \eta + \theta + \delta$.

B. Conserved lattice gas model

In the CLG model, each lattice site can be occupied by at most one particle; the particle is considered active if at least one of its neighboring sites is occupied by another particle. If all the neighboring sites are either empty or fully occupied, the particle is considered inactive. Initially, ρL^d particles are distributed on a d -dimensional cubic lattice of side L . Each particle is then determined if it is active or inactive, and active particles are stored on the list. As dynamics proceed, the mean and mean-squared densities of activity are sampled by the same way as for the Manna model.

A number of researchers have studied the critical behavior using the initial states with a random distribution of particles. In one dimension, the hopping is known to be deterministic on a chain because each active particle has a single empty site, and the deterministic hopping is known to yield a critical behavior different from that of the Manna model [35,36]. However, on a finite-width stripe and in higher dimensions the hopping is stochastic, and the CLG model has been known to exhibit the same critical behavior as the Manna model.

C. Preparation of initial states

In this subsection, we briefly describe how the initial states are prepared in the MC simulations.

Random initial states. The simplest way of obtaining an initial state is to randomly distribute ρL^d particles, and each lattice site is then analyzed if it is either active or inactive following the rule of the model. Particles on inactive sites do not participate actively at the current time, but they become active at later times by the activity of particles on the neighboring

sites. The role of the background particles is thus nontrivial on the critical behavior of activities.

Natural initial states. The natural initial states are described in Ref. [16]. Starting from a random distribution of particles, let the dynamics continue until random initial fluctuations are sufficiently smoothed out, i.e., until the time of the cumulative density of particles becomes stationary, and then the system is reactivated by allowing all particles to diffuse in a single MC sweep. Apparently the decay of activity for the NISs is much faster than that for the RISs because particle distribution for NISs is close to that of the steady state or absorbing state, and this yields a larger decay exponent. The distribution of particles is known to be random on a short scale and is hyperuniform on a larger scale [25,26].

Uniform initial states (UISs). In contrast to the NISs, particles are initially distributed uniformly, with the inter-particle distance $(1/\rho)^{1/d}$ in a d -dimensional lattice; in one dimension, the position of the i th particle is $x(i) = \text{int}(i/\rho)$. In higher dimensions, we create a uniform distribution of particles on a chain of length L^d and divide the chain into L^{d-1} shorter chains of length L . We then assemble orderly the shorter chains to create a d -dimensional lattice. The coordinate of the i th particle in d dimensions is

$$\mathbf{x}_k(i) = \frac{1}{L^{d-k}} \left[\text{int}(i/\rho) - \sum_{j=1}^{k-1} \mathbf{x}_j L^{d-j} \right], \quad (1)$$

where $\mathbf{x}_k(i)$ is the k th coordinate of the i th particle. To produce active sites, an MC sweep is taken; i.e., all particles are moved a single step to the nearest-neighbor sites selected at random. In this initial state, the correlation length among particles is very short and does not exceed few lattice constants, and the distribution of background particles is uniform. The initial decay of activity density depends on the initial states for a short time, but the asymptotic critical behavior for NISs and UISs should remain the same. On the other hand for the RISs, the exponents associated with dynamics of the system such as the decay exponent θ and dynamic exponent z are known to differ from those of the homogeneous initial states.

D. Spatial correlations

Recently, an alternative method for measuring correlation length on the surface models was introduced by one of us [4]. Here, we apply it to Manna models and describe the way of measuring the correlation length briefly. We consider relative variance of activity $\sigma/\langle\rho_a\rangle$ to be proportional to $1/\sqrt{N}$, where $\sigma = (\langle\rho_a^2\rangle - \langle\rho_a\rangle^2)^{1/2}$ and N is the independent number of samples. When the correlation length $\xi(t)$ is small compared to the system size L , ρ_a is effectively averaged over $(L/\xi)^d$ independent samples, i.e., $\sigma/\langle\rho_a\rangle \sim 1/\sqrt{N} \sim (\xi/L)^{d/2}$, or equivalently, $\xi(t) \sim L(\sigma^2/\langle\rho_a\rangle^2)^{1/d}$. Thus, the quantity $R(L, t)$ is proportional to the correlation length, i.e.,

$$R(t, L, \Delta) = L \left(\frac{\langle\rho_a^2\rangle - \langle\rho_a\rangle^2}{\langle\rho_a\rangle^2} \right)^{1/d} \sim \xi(L, t), \quad (2)$$

where the mean activity density $\langle\rho_a\rangle$ is identical to $\rho_a(t, L, \Delta)$. The correlation length can thus be calculated from the fluctuation of $\rho_a(t, L, \Delta)$. The data of $R(t, L, \Delta)$ for

sufficiently large systems at ρ_c behave as $R(t) \sim t^{1/z}$, which enables one to measure the dynamic exponent [4].

Assuming $R(t, L, \Delta)$ to be a homogeneous function, the scaling theory allows one to write

$$R(t, L) = t^{1/z} F(t/b^z, L/b) = L \mathcal{F}(t/L^z) \quad (3)$$

at $\Delta = 0$, where b is the scaling factor. On the other hand, for a sufficiently large system of $L \gg \xi$,

$$R(t, \Delta) = t^{1/z} G(\Delta b^{1/\nu_\perp}, t/b^z) = \Delta^{-\nu_\perp} \mathcal{G}(\Delta t^{1/\nu_\parallel}). \quad (4)$$

As $t \rightarrow \infty$, $R(t, \Delta) \rightarrow R_{\text{sat}}(\Delta) \sim \Delta^{-\nu_\perp}$, and therefore, one can calculate the correlation-length exponent ν_\perp by plotting R_{sat} against Δ on a double logarithmic scale. Using the critical exponent associated with fluctuation of activity

$$\chi(\rho_a) = L^d (\langle \rho_a^2 \rangle - \langle \rho_a \rangle^2) \sim \Delta^{-\gamma} \quad (5)$$

in Eq. (2), the known scaling relation $\gamma + 2\beta = d\nu_\perp$ [18] is attained from Eq. (4).

III. RESULTS AND DISCUSSION

The primary purpose of this paper is to measure the critical exponents associated with correlation lengths from the numerical data of $R(t, L, \Delta)$ for the Manna and CLG models. An advantage of using $R(t)$ is that, in addition to direct measurements of the correlation lengths, the method may be used to validate the critical point estimated by the conventional methods particularly when the activity density decays slowly in time. The critical point has been determined from the best power laws of $\rho_a(t)$ and $\rho_{\text{sat}}(\Delta)$, and all the critical exponents will be unreliable if the value of ρ_c is poorly determined; the data of $R(t)$ may thus be used as an alternative method to validate the value of ρ_c . It should be noted that the data of $R(t)$ are much noisier than those of $\rho_a(t)$, and therefore, the sample size should be much larger. The data presented here are the averages of at least 2×10^3 independent samples for larger systems and more for smaller systems.

We first present our simulation results for the Manna model in two dimensions using both the NISs and UISs to validate the known value of ρ_c and calculate the correlation-length exponents. We also show that the critical exponents calculated using the two initial states are the same, provided that the homogeneity of particle distribution is properly achieved. We then present new results for the Manna model using UISs and the CLG model using NISs in three dimensions. The two models are expected to exhibit the same critical behavior; therefore, the results will serve for a consistency check. (Note that the reported results in three dimensions were those from RISs, and the correct critical exponents from homogeneous initial states do not yet exist.) The delicate and controversial Manna model in one dimension is discussed in the last subsection.

A. Manna model in two dimensions

The critical behavior of the Manna model was first studied in [18] using RISs, and the critical density was estimated as $\rho_c = 0.68333(3)$. More recently, one of us extensively studied this, employing both NISs and RISs [32], and the value of ρ_c was found to be $\rho_c = 0.68354$ from the power laws of

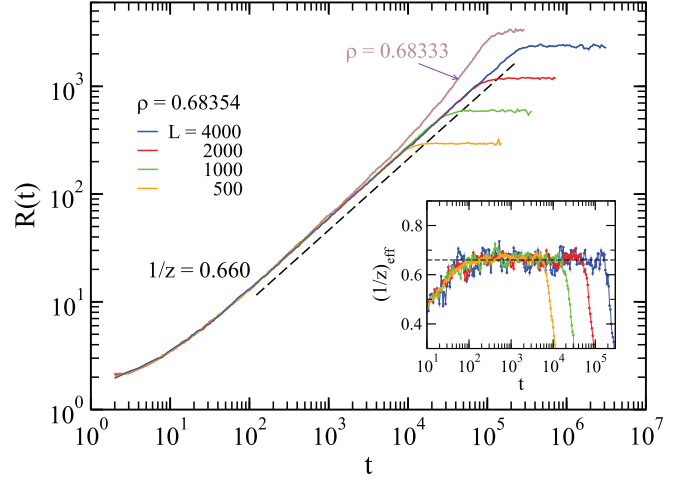


FIG. 1. The surviving-sample average data of $R(t)$ for the Manna model on a square lattice calculated using NISs at $\rho = 0.68354$ for systems of selected sizes, in comparison with the data at the reported critical density of $\rho = 0.68333$ [18]. The dashed line is the power-law fit over the data for $L = 4000$, giving the inverse dynamic exponent $1/z = 0.660$. The inset shows the effective exponents of $1/z$ defined in Eq. (6) calculated using the data in the main panel. The horizontal dashed line is the mean of the data for $L = 4000$ within the fitting region.

$\rho_a(t)$ and $\rho_{\text{sat}}(\Delta)$ on a square lattice of $L = 6000$. The critical exponents θ , β , and β/ν_\perp were measured directly from the numerical data and ν_\perp and ν_\parallel indirectly using the scaling relations.

To validate our method, we carried out simulations on systems of sizes $L = 500, 1000, 2000$, and 4000 at $\rho_c = 0.68354$ using NISs and calculated the data of $R(t_k, L)$. The results were compared with the data for $\rho = 0.68333$ on a system of $L = 4000$; Fig. 1 shows the data of $R(t, L)$ averaged over those samples which survive up to the time t (surviving samples). The data for $\rho_c = 0.68354$ exhibit a clean power-law behavior for all sizes and saturate to steady-state densities as $t \rightarrow \infty$, supporting that the known critical point is accurate, whereas data for $\rho = 0.68333$ show an upward curvature suggesting it to be subcritical. The saturating behavior at ρ_c is the finite-size effect reflected from the saturation of activity on a finite system. As the size of system increases, the power-law region increases, and in the limit of $L \rightarrow \infty$, the saturating behavior is expected to diminish. On the other hand, the data averaged over all samples (all-sample averages), including those which survive up to time t and those which fall into absorbing states, differ near and at ρ_c and diverge rather than saturate. (Comparison of the two averages will be presented in the subsequent subsection for the CLG model in three dimensions.) The inset shows the effective exponents, defined by

$$(1/z)_{\text{eff}} = \frac{\log_{10}[R(t_{k+n}, L)/R(t_k, L)]}{\log_{10}[t_{k+n}/t_k]} \quad (6)$$

calculated using $n = 50$, which are equivalent to the local slopes between the two points separated by $\Delta(\log_{10} t) \approx 1$ on a double logarithmic scale. The mean of the data within the power-law region marked by the dashed line in the main

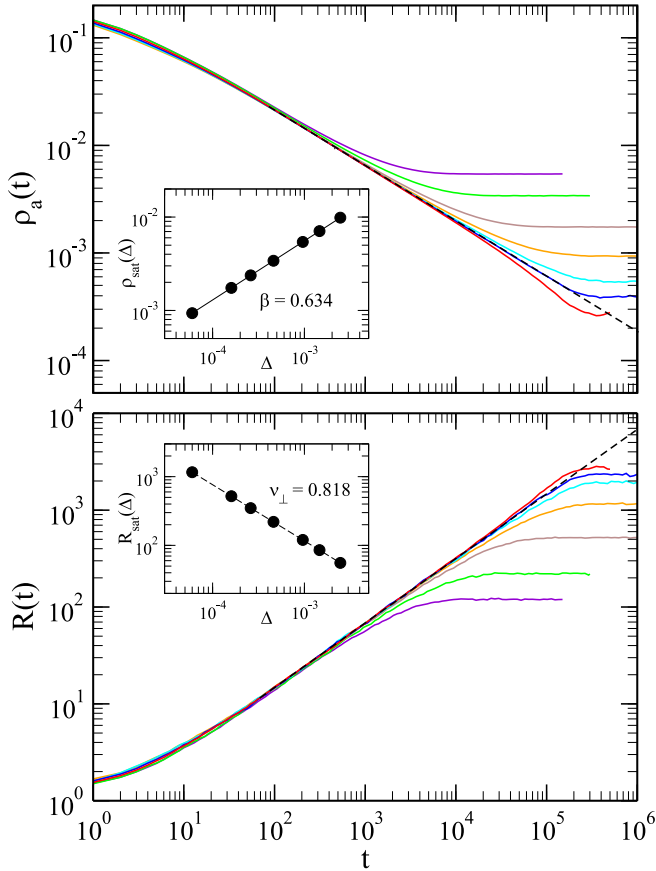


FIG. 2. The surviving-sample average data of $\rho_a(t)$ (top) and $R(t)$ (bottom) for the Manna model on a square lattice of $L = 4000$ calculated using UISs for particle densities of, from bottom to top for $\rho_a(t)$ and from top to bottom for $R(t)$, $\rho = 0.68352, 0.68354, 0.68356, 0.6836, 0.6837, 0.684, \text{ and } 0.6845$. The two data sets below and above $\rho_c = 0.68354$ are deviated toward the opposite directions from the power laws in both plots, and the dashed lines are the power-law fits over the data for ρ_c . Plotted in the inset are the steady-state values against the distance from criticality.

panel is $1/z = 0.660(7)$, giving the dynamic exponent $z = 1.515(16)$. The error of $1/z$ is the standard deviation of $(1/z)_{\text{eff}}$ values for $L = 4000$.

In order to show that the two homogeneous initial states, NISs and UISs, yield the same critical exponents, we also carried out simulations using the UISs. In Fig. 2, the upper plots show the data for $\rho_a(t)$ and the lower one for $R(t)$, for the same selected particle densities on a system of $L = 4000$. In both plots the data for the two selected densities below and above ρ_c , i.e., for $\rho = 0.68352$ and 0.68356 , deviate toward the opposite directions from the power laws, indicating that the UISs give the same critical density when determined from the power laws of $\rho_a(t)$ and $R(t)$. The saturating behavior of the subcritical data for $\rho = 0.68352$ in the long-time limit is reflected from the saturation of activity for a finite system by fluctuation.

The power-law plots over the data for ρ_c yield the critical exponents $\theta = 0.515(8)$ and $1/z = 0.667(4)$, the errors of which were determined from the standard deviations of the effective exponents θ_{eff} and $(1/z)_{\text{eff}}$, the former of which is

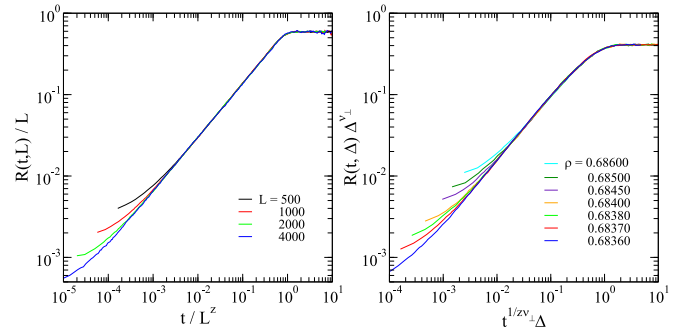


FIG. 3. The finite-size scaling plot of Eq. (3) (left) and off-critical scaling plot of Eq. (4) (right) for the data in Fig. 2, using the estimates $\rho_c = 0.68354$, $z = 1.50$, $\nu_{\perp} = 0.818$.

defined by replacing $R(t_k) \rightarrow \rho_a(t_k)$ and taking the negative in Eq. (6). The insets are the plots of the steady-state values against Δ , with the associated critical exponents $\beta = 0.634(3)$ and $\nu_{\perp} = 0.818(3)$. The errors were estimated from the variations of the estimates by shifting the fitting regions, and there might be additional statistical errors not accounted for. The estimates of θ and β are consistent with those of [32], whereas the dynamic exponent $z = 1.50(1)$ and correlation-length exponent ν_{\perp} are slightly different. While in [32] the values of z and ν_{\perp} were estimated from the finite-size and off-critical scalings of $\rho_a(t, \Delta, L)$ and scaling relations, in this paper we directly measured them using the values of $R(t, \Delta, L)$. We therefore believe that our estimates are more reliable with smaller errors.

The data of $R(t, L, \Delta)$ in Figs. 1 and 2 were analyzed by finite-size scaling and off-critical scaling using the estimated critical exponents; the left plot of Fig. 3 is the finite-size scaling data and the right plot the off-critical scaling data. In both plots, the scaled data collapse onto a single curve in the asymptotes. It should be noted that data for $\rho = 0.68356$ and 0.68358 were not plotted in the off-critical scaling plot because those data did not collapse due to the finite-size effect near criticality.

We have shown that the two homogeneous initial states, NISs and UISs, yielded the same critical behavior. In practice, the UISs are much more efficient than NISs because UISs do not require a prerun to homogenize the particle distribution or need verification of homogeneity of the particle distribution.

B. Manna model and conserved lattice gas model in three dimensions

In this subsection, we present the results for the APT critical behaviors of the Manna and CLG models using homogeneous initial states, i.e., UISs for the Manna model and NISs for the CLG model. Because the main interest lies in whether the different critical behavior for the Manna model is a perturbation of the DP critical behavior, researchers have paid attention in lower dimensions. In higher dimensions, i.e., in three dimensions, the critical exponents in the Manna and DP classes are not expected to be very different because three dimensions are closer to the upper critical dimension $d_c = 4$ of both universality classes at which all the critical exponents remain the same. Therefore, the critical behavior in three

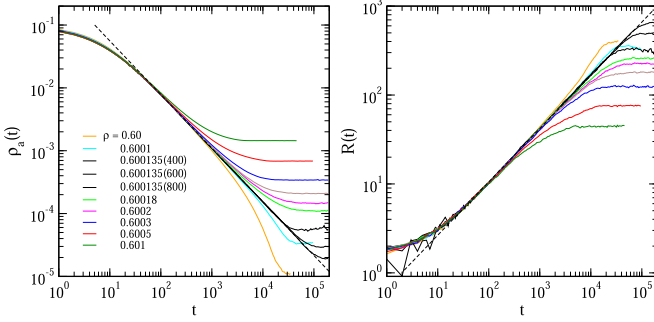


FIG. 4. Data of $\rho_a(t)$ (left) and $R(t)$ (right) calculated for the Manna model in three dimensions using UISs for the selected particle densities on systems of $L = 400, 600,$ and 800 for $\rho = 0.600135$ (black lines) and $L = 400$ for other values of ρ . The legends are of the same order as the data from bottom to top for $\rho_a(t)$ and from top to bottom for $R(t)$. The dashed line in each plot is the power-law fit over the data of ρ_c .

dimensions is far from researchers' interest, and the results using the homogeneous initial states to be presented here are new.

1. Manna model using UISs

The stochastic Manna model in three dimensions was studied decades ago by Lübeck and Heger, and the critical density was found to be $\rho_c = 0.60018(4)$ [18]. We calculated $R(t)$ and $\rho_a(t)$ for various values of ρ close to and above the known value of ρ_c to validate the critical density. The critical exponents are then calculated at the critical point. Figure 4 shows the data for $\rho_a(t)$ (left) and $R(t)$ (right) calculated on systems of $L = 400, 600,$ and 800 for $\rho = 0.600135$ and $L = 400$ for other values of ρ . From both plots, it is clear that data show clean power-law behavior at $\rho = 0.600135$ and the power-law region becomes wider as the size of the system increases, indicating $\rho_c = 0.600135$. The data of other values of ρ deviating from the power law also support the value of ρ_c , that is close to but slightly smaller than the value reported in Ref. [18]. The power-law plots yield the critical exponents $\theta = 0.850(6)$ and $1/z = 0.601(7)$, or equivalently, $z = 1.66(2)$. The steady-state values of $\rho(t)$ and $R(t)$, $\rho_{\text{sat}}(\Delta)$ and $R_{\text{sat}}(\Delta)$, also yielded the power-law behaviors, with the powers of $\beta = 0.870(3)$ and $\nu_{\perp} = 0.628(4)$ (not shown). The exponents associated with dynamics θ and z are very different from the known values, $\theta = 0.745(17)$ and $z = 1.823(23)$, calculated using the data of RISs [18], as expected for different initial states. The static exponents β and ν_{\perp} also differ slightly from the reported values, $\beta = 0.840(12)$ and $\nu_{\perp} = 0.593(13)$. In the earlier study, the numerical data were obtained using relatively smaller systems with limiting facilities decades ago, and we believe that our results are more reliable.

2. CLG model using NISs

The CLG model in three dimensions was studied by Lübeck and a collaborator [11,18] and more recently by one of us [32], all using RISs, before the issue of different initial states was raised in [16]. Because the steady-state values of

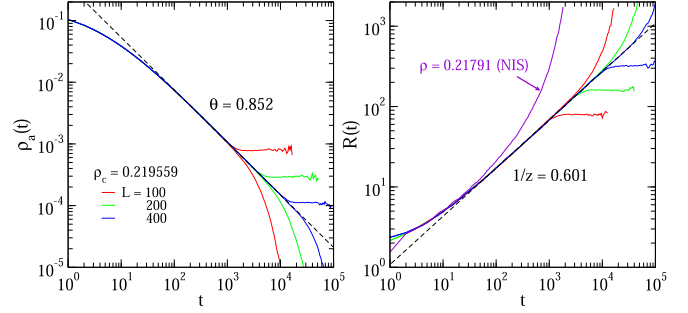


FIG. 5. Data of $\rho_a(t)$ (left) and $R(t)$ (right) for the CLG model in three dimensions, both calculated at the critical density of $\rho = 0.219559$ for systems of three selected sizes. The decaying data on the left and diverging data on the right are the all-sample averages and the saturating data are the surviving-sample averages. The data for $\rho = 0.21791$ are the averages over surviving samples. The dashed line in each plot is the power-law behavior, with the power given in each plot.

activity remain the same for various initial states, the static critical exponents as well as the critical density should remain the same. The critical density of particles estimated in [11] and [18] was $\rho_c = 0.21791$, whereas in [32] it was $\rho_c = 0.219559$. In Ref. [11], the critical density was estimated as follows: first let the simulation run until the system reaches a steady state, and then the steady-state density $\langle \rho_{\text{sat}} \rangle$ was calculated on systems of $L = 16 \sim 160$. Close to the transition point, 5×10^6 update steps were performed to reach the steady state for the largest system of $L = 160$ and the density of active sites was monitored for the next 5×10^5 update steps. The critical density was determined from the best straight line of $\langle \rho_{\text{sat}} \rangle$ versus $\rho - \rho_c$ on a double logarithmic scale, assuming ρ_c as a trial value. In this procedure, the surviving-sample averages appeared to have been used, and those samples that survive up to the time of steady states must have been considered supercritical. Close to the transition point on finite-size systems, the number of subcritical samples may also survive by fluctuation up to the time for steady states; thus, the critical point appeared to have been significantly underestimated. Our data of $R(t)$ show that the critical density reported in [11] is indeed subcritical.

We calculated $R(t, L, \Delta)$ using $\rho = 0.21791$ on a cubic system of $L = 400$ and the more recent value of $\rho_c = 0.219559$ on systems of $L = 100, 200,$ and 400 , both using NISs. Plotted in Fig. 5 are the data of $\rho_a(t)$ (left) and $R(t)$ (right); the decaying data of $\rho_a(t)$ and the diverging data of $R(t)$ are the all-sample averages and the saturating data are the surviving-sample averages. The two types of averages differ in the large- t limit due to the finite-size effect. The diverging surviving-sample averages of $R(t)$ for $\rho = 0.21791$ show that the earlier estimate of ρ_c is much smaller than the true value. On the other hand, for $\rho_c = 0.219559$, the data for both $\rho_a(t)$ and $R(t)$ show good power laws, with wider power-law regions for larger system sizes. The power-law exponents are calculated from the data within the region in which the two types of samples coincide to eliminate the finite-size effect. From the power-law fits, the critical exponents $\theta = 0.848(3)$ and $1/z = 0.601(6)$ or $z = 1.66(2)$ were obtained.

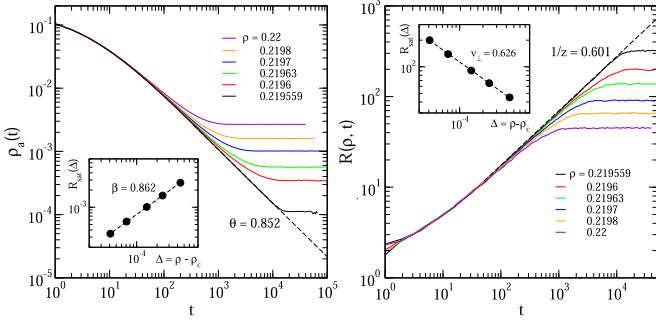


FIG. 6. Data of $\rho_a(t)$ (left) and $R(t)$ (right) for selected values of ρ in the CLG model on a system of $L = 400$ in three dimensions. The dashed lines are the power-law fits over the data for $\rho_c = 0.21959$. Plotted in the inset are the steady-state values against Δ , with the dashed lines being the power-law fits over the data.

The values of $\rho_a(t, \Delta)$ and $R(t, \Delta)$ were also calculated for selected values of ρ on a system of size $L = 400$ and the results are plotted in Fig. 6; the insets are the plots of the steady-state values against Δ , yielding $\beta = 0.862(5)$ and $\nu_{\perp} = 0.626(4)$, which are consistent with the earlier estimates obtained using RISs. (Note that both are the static exponents that are expected to be irrespective of the initial states.) With the estimated values, $\nu_{\parallel} = \beta/\theta = 1.01(1)$ is consistent with the value $\nu_{\parallel} = z\nu_{\perp} = 1.04(2)$ within errors. The estimates for the Manna and CLG models in three dimensions are summarized and compared with those of the DP class in Table I; it is clear from the data that the two models belong to the same universality class that is distinct from the DP class.

C. Manna model in one dimension

The Manna model in one dimension is the simplest model in the Manna universality class, and researchers have studied this model using various initial states. Although the asymptotic critical behavior is expected to remain the same for NISs and RISs, the reported critical density of activity and critical exponents scattered depend on the authors; even the results from NISs also differed. The results for NISs and UISs reported in the literature are summarized in Table II.

In order to examine the cause of such inconsistency, we first carried out simulations on a system of a linear size $L = 2 \times 10^5$ for the reported critical densities using both RISs and NISs: for $\rho = 0.89236$ [16] and 0.89216 [32] up to $t = 10^7$ and for $\rho = 0.89252$ [29] up to $t = 10^8$. The RIS data were sampled after preruns of up to the largest assigned time

TABLE I. The estimates of the critical exponents for the Manna and CLG models in three dimensions using the homogeneous initial states, in comparison with those of the DP class.

	θ	z	β	ν_{\perp}	ν_{\parallel}
Manna	0.850(6)	1.66(2)	0.870(3)	0.628(4)	1.03(2)
CLG	0.852(3)	1.66(2)	0.862(5)	0.626(4)	1.04(3)
DP ^a	0.732(4)	1.90(1)	0.813(11)	0.581(5)	1.105(5)

^aReference [2].

TABLE II. Summary of the critical exponents for the Manna model in one dimension, in comparison with the present estimates and DP values. The upper three sets are for the NISs and the fourth set for the UISs.

	ρ_c	θ	β	ν_{\parallel}	z	ν_{\perp}
Ref. [16]	0.89236(3)	0.159(3)	<0.31	1.75(5)	1.51(5)	1.095(5)
Ref. [27]	0.89216(3)	0.158	0.380(5)	2.405		
Ref. [28]	0.89255(2)	0.146(2)	0.278(2)	1.9(1)	1.73(18)	1.10(15)
Ref. [29]	0.89252(5)	0.162(3)	0.311(6)	1.92	1.32	1.450(5)
This work	0.89255(3)	0.148(2)	0.30(1)	1.80(2)	1.50(2)	1.198(3)
DP values ^a		0.1594	0.2764	1.733	1.5807	1.0969

^aReference [2].

steps, and afterward, the homogeneous NISs were prepared by sweeping all particles to diffuse a single MC step. Although 10^7 prerun time steps might be insufficient to homogenize the distribution for the first two cases, we realize that the cumulative particle density was found to be leveled out after 10^8 time steps for the last case [27]. Figure 7 shows the data for $R(t)$; the upper set is for NISs and the lower set for RISs. From the plots, we realize that none of the data using the NISs yield a power-law behavior, suggesting that the sampled data may not be sufficient to calculate the critical exponents. For $\rho = 0.89252$, even though the cumulative densities of particles were found to be stationary after $t = 10^8$ steps, the assigned prerun time steps appear to be insufficient to homogenize the distribution of particles. This may be supported from the hyperuniformity, defined by the fluctuation of density of particles within a window of size ℓ , $\langle \rho_{\ell}^2 \rangle - \langle \rho_{\ell} \rangle^2 = \ell^{-\chi}$. The hyperuniformity exponent of the steady-state particle distribution in the one-dimensional Manna model is known to be $\chi \approx 1.425$ [25], indicating that the distribution is hyperuniform but not perfectly uniform; if the distribution is uniform, the value of χ will essentially be infinity. Thus,

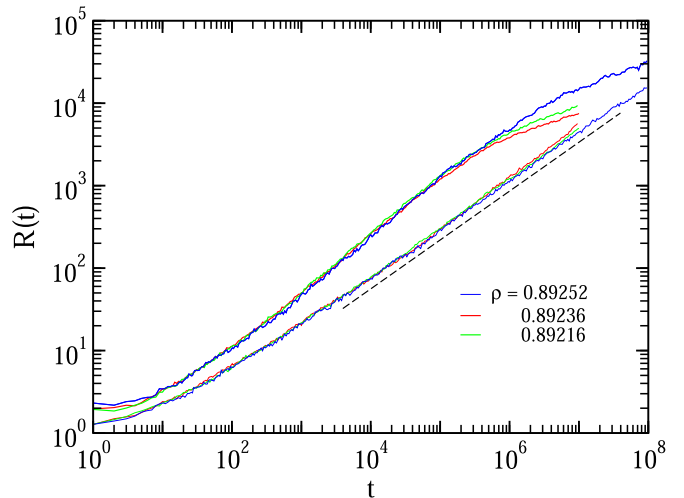


FIG. 7. Data of $R(t)$ defined in Eq. (2) for the Manna model in one dimension, calculated on a system of $L = 2 \times 10^5$ using NISs (upper set) and RISs (lower set) for the reported values of the critical exponent.

inactive background particles are still correlated, and such correlation may lead nontrivial effects to the critical behavior in one dimension, whereas it does not appear to affect the critical behavior in higher dimensions. The slow decay of activity during preruns, i.e., small decay exponent for RISs (<0.15 [18]), requires a large number of prerun time steps to homogenize the distribution in one dimension. As the time step increases, the correlation length also increases in time and may exceed the system size; thus, the employed system size may not be large enough to eliminate the size effect. In higher dimensions, on the other hand, the decay of activity with larger decay exponent (>0.45) appears to yield correlation rapidly dying out. Neglecting these subtleties, the value of ρ_c determined from the best power laws of $\rho_a(t)$ and $\rho_{\text{sat}}(\Delta)$ appeared to differ depending on the authors in one dimension, and accordingly, the critical exponents also differed. This might be the cause of the scattered values of ρ_c and critical exponents. The data of $R(t)$ from RISs, on the other hand, exhibit fairly good power-law behavior for $\rho = 0.89252$ as shown with a dashed line in Fig. 7, whereas data for the other two values were about to deviate upward, suggesting that $\rho = 0.89252$ is close to the critical density and the other two values are subcritical. The power, however, gives a wrong value of $1/z \approx 0.59$ that may yield a scaling anomaly, as explained in Sec. I.

Because the static critical exponents such as β and ν_\perp remain unchanged for different initial states as was explained in Sec. I and found in two dimensions, the critical density should also remain the same for different initial states. In addition, the critical exponents for NISs and UISs should be the same, provided that the particle distribution is properly homogenized. With this expectation, a simple way to avoid subtleties on homogenization discussed earlier is to employ the UISs. We therefore carried out simulations using UISs on a system of size $L = 3 \times 10^5$ up to $t = 3 \times 10^7$. Plotted in Fig. 8 are the data of $\rho_a(t)$ (upper plots) and $R(t)$ (lower plots) for five selected values of ρ very close to ρ_c at which those data are expected to show the best power-law behaviors in the asymptotes. However, the local slopes of both the data of $\rho(t)$ and $R(t)$ plotted on a double logarithmic scale vary slowly, making it difficult to estimate the powers. Focusing on the data in the asymptotic limit, it appears that the best power laws are observed for $\rho_c = 0.89255$. The effective exponents were calculated from the data of both $\rho_a(t)$ and $R(t)$ generated at ρ_c and the results obtained using $n = 10$ were plotted in the smaller insets. (Note that a smaller value of n was used to reflect slowly varying local slopes.) The effective exponents indeed vary in time and become stationary for $t > 5 \times 10^5$ as marked with arrows; thus the critical exponents should be estimated in this region and they are $\theta = 0.148(2)$ and $1/z = 0.666(10)$, the errors of which are the standard deviations of the effective exponents. If the decreasing trend of θ_{eff} is assumed for longer time steps, the value of θ will be even smaller and farther from the DP value and the value of [16]. The smaller estimate of θ than that in [16] appears to be attributable to a larger value of ρ_c . Plotted in the larger insets are the steady-state values as a function of Δ . [Note that the original data of $\rho_a(t)$ and $R(t)$ were not shown in the main panel.] The power-law fits yield $\beta = 0.30(1)$ and $\nu_\perp = 1.198(3)$. It is worth emphasizing that the value of β

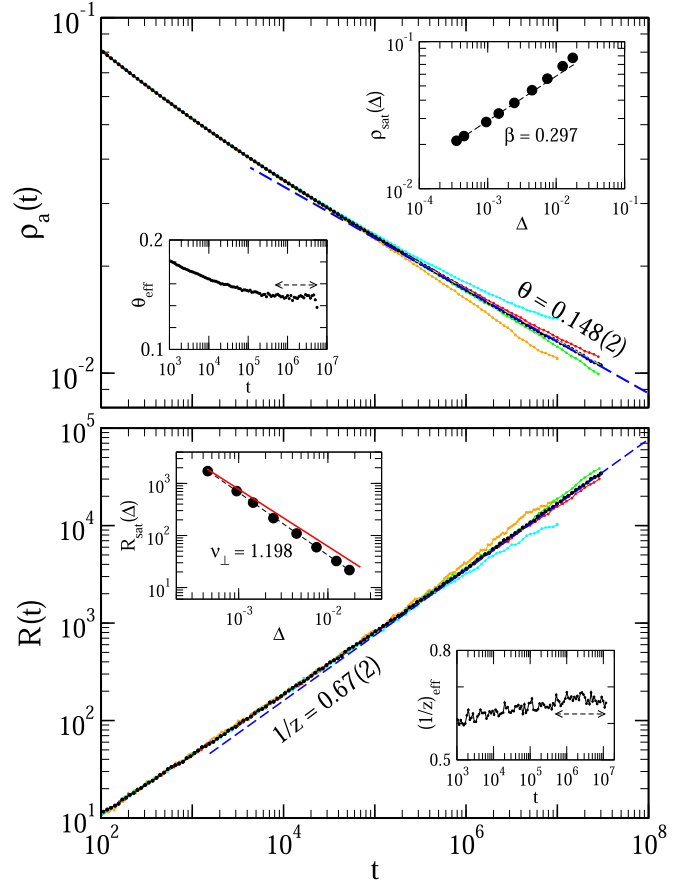


FIG. 8. Data of $\rho_a(t)$ (upper plots) and $R(t)$ (lower plots) for five selected particle densities for, from bottom to top in the upper plot and from top to bottom in the lower plot, $\rho = 0.8925, 0.89254, 0.89255, 0.89256, \text{ and } 0.8926$. Data for $\rho_c = 0.89255$ show the best power-law behaviors in both plots. Plotted in the smaller insets are the local slopes defined in a similar way to Eq. (6) calculated using the data in the main panels. The critical exponents and errors were estimated from the data within the regions marked by the arrows. The data in the larger insets are the steady-state values of $\rho_a(t)$ and $R(t)$, and the red solid line is for comparison with the DP value.

is less reliable because data of ρ_{sat} yield curvature and may become smaller if the data of smaller Δ are sampled. On the other hand, data for $R_{\text{sat}}(\Delta)$ exhibit a good power-law behavior and yield the power which is larger than the DP value. If the value of ν_\perp for the Manna model is compatible to the DP value, the data of R_{sat} should lie on the red solid line or, at least, fluctuate around the line; however, it is not likely. If the power-law fitting is examined with a smaller value of ρ_c such that the estimate of θ is close to the DP value (as in [16]), the value of ν_\perp will become larger and the data will deviate farther from the DP line. In Ref. [28], the authors obtained $\beta = 0.278(2)$ and $\nu_\perp = 1.1(1)$, both of which were consistent with the DP values and, with these values, they favored the DP universality class, despite the exponents associated with dynamics depending on the initial states. However, the plot of $R_{\text{sat}}(\Delta)$ appears to rule out such a possibility. The finite-size scaling and off-critical scaling of the data for $R(t, L, \Delta)$ in Fig. 9 confirm our estimates.

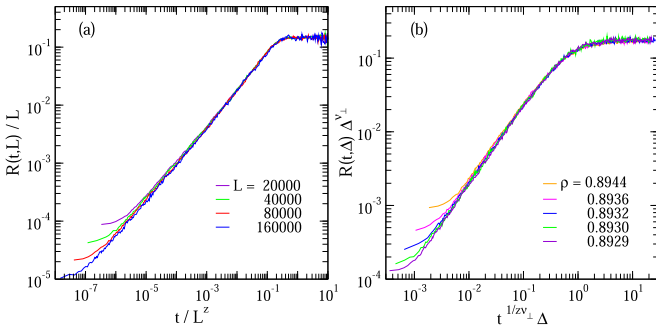


FIG. 9. Data for the (a) finite-size scaling of Eq. (3) and (b) off-critical scaling of Eq. (4) for the data of $R(t)$ in the Manna model in one dimension. Data for various size systems collapse in (a) and those for different particle-densities fall onto a single curve in the asymptotes in (b), when scaled with the estimated critical exponents of $\nu_{\perp} = 1.198$ and $1/z = 0.666$. In (b) the chosen system sizes $L > 10 \times (\rho - \rho_c)^{-\nu_{\perp}}$ were found to be sufficient to eliminate the finite-size effect.

IV. SUMMARY AND CONCLUSIONS

We have studied APT critical behavior for the models in the Manna class in one, two, and three dimensions, by employing an alternative method for measuring correlation lengths coupled with a conventional method, using the two types of homogeneous initial states. We have calculated $R(t, L, \Delta)$ by MC simulations that is directly proportional to the spatial correlation lengths for the Manna and CLG models using NISs and UISs. The two initial states are expected to yield the same critical behaviors provided that the initial particle distribution is successfully homogenized.

In two dimensions, we have shown that data for $R(t, L, \Delta)$ in the Manna model from the two initial states yielded consistent critical exponents. In three dimensions, we presented the critical exponents for the Manna model using UISs and CLG model using NISs. The critical exponents of the two models were found to be consistent, indicating that the two models belong to the same universality class and the two initial states yield the same critical behavior. The estimates however differed from the values in the DP class.

We finally discussed controversial critical behavior of the Manna model in one dimension. In the Manna model in one dimension, the known critical density varied depending on the authors; as a result, the critical exponents were scattered. We first carried out MC simulations and calculated $R(t)$ for the known critical densities using both RIS and NIS and

found that none of the data for the known critical densities exhibited the power-law behavior $R(t) \sim t^{1/z}$ when NISs were employed. On the other hand, data from RISs yielded a good power-law behavior for $\rho = 0.89252$, and those for $\rho = 0.89233$ and $\rho = 0.89215$ deviated. This observation is contrasted to that in higher dimensions where $R(t)$ for both RISs and NISs yielded power-law behaviors at criticality but with different powers. The cause of such an anomalous behavior was conjectured to be attributable to the correlations among background particles. Although the homogeneity of the distribution of inactive background particles has been examined by cumulative density fluctuation in the earlier works, the background particles seemed to have been still correlated in one dimension. We further studied the model using UISs in which the correlations among background particles die out within few lattice constants. The critical exponents estimated from the data of $R(t, \Delta)$, $1/z \simeq 0.66$, and $\nu_{\perp} \simeq 1.20$ differed slightly from the DP values of $1/z \simeq 0.63$ and $\nu_{\perp} \simeq 1.1$. Although the difference is not large enough for classification of different universality classes, the data of $R_{\text{sat}}(\Delta)$ appeared not likely to follow the fitting line that is compatible to the DP value. Considering this observation and together with the results in higher dimensions, we concluded that the Manna model belongs to the universality class that is distinct from the DP class and the Manna universality class is an independent class.

We have shown that $R(t)$ effectively gives critical exponents associated with correlation lengths that are consistent with those which were obtained from the conventional methods. Summarizing the advantages of using $R(t)$, it gives a power-law behavior at the critical point; therefore, the data of $R(t)$ may serve to accurately determine the critical point, or at least, they can serve as an alternative method. $R(t)$ at the critical point and $R_{\text{sat}}(\Delta)$ in the supercritical region enable one to measure directly the dynamic exponent and spatial correlation-length exponent. The data of $R(t)$ may also provide relevant information on the finite-size and crossover behaviors at or near the critical point. We believe that similar analysis can be applicable to other related problems in the critical phenomena.

ACKNOWLEDGMENTS

We would like to thank S. J. Kim for numerical help. This research was supported by a grant from the National Research Foundation of Korea (Grant No. NRF-2020R1A2C1003971) and by the Basic Science Research Program funded by the Ministry of Education (Grant No. NRF-2021R1A6A1A03043957).

- [1] J. Marro and R. Dickman, *Nonequilibrium Phase Transition in Lattice Models* (Cambridge University Press, Cambridge, 1999).
- [2] H. Hinrichsen, Non-equilibrium critical phenomena and phase transitions into absorbing states, *Adv. Phys.* **49**, 815 (2000); G. Ódor, Universality classes in nonequilibrium lattice systems, *Rev. Mod. Phys.* **76**, 663 (2004).
- [3] S. Lübeck, Universal scaling behavior of non-equilibrium phase transitions, *Int. J. Mod. Phys. B* **18**, 3977 (2004).
- [4] J. M. Kim, A new way of measuring the correlation length in surface growth models, *J. Stat. Mech.* (2021) 033213.
- [5] R. Dickman, A. Vespignani, and S. Zapperi, Self-organized criticality as an absorbing-state phase transition, *Phys. Rev. E* **57**, 5095 (1998).
- [6] A. Vespignani, R. Dickman, M. A. Muñoz, and S. Zapperi, Driving, Conservation, and Absorbing States in Sandpiles, *Phys. Rev. Lett.* **81**, 5676 (1998).

- [7] A. Vespignani, R. Dickman, M. A. Muñoz, and S. Zapperi, Absorbing-state phase transitions in fixed-energy sandpiles, *Phys. Rev. E* **62**, 4564 (2000).
- [8] J. F. F. Mendes, R. Dickman, M. Henkel, and M. C. Marques, Generalized scaling for models with multiple absorbing states, *J. Phys. A: Math. Gen.* **27**, 3019 (1994).
- [9] S. Lübeck, Scaling behavior of the conserved transfer threshold process, *Phys. Rev. E* **66**, 046114 (2002).
- [10] M. Rossi, R. Pastor-Satorras, and A. Vespignani, Universality Class of Absorbing Phase Transitions with a Conserved Field, *Phys. Rev. Lett.* **85**, 1803 (2000).
- [11] S. Lübeck, Scaling behavior of the absorbing phase transition in a conserved lattice gas around the upper critical dimension, *Phys. Rev. E* **64**, 016123 (2001).
- [12] S. Lübeck, Scaling behavior of the order parameter and its conjugated field in an absorbing phase transition around the upper critical dimension, *Phys. Rev. E* **65**, 046150 (2002).
- [13] F. van Wijland, K. Oerding, and H. J. Hilhorst, Wilson renormalization of a reaction-diffusion process, *Physica A* **251**, 179 (1998).
- [14] R. Pastor-Satorras and A. Vespignani, Field theory of absorbing phase transitions with a nondiffusive conserved field, *Phys. Rev. E* **62**, R5875 (2000).
- [15] S. Kwon and Y. Kim, Dynamical scaling behavior of the one-dimensional conserved directed-percolation universality class, *Phys. Rev. E* **85**, 051119 (2012).
- [16] M. Basu, U. Basu, S. Bondyopadhyay, P. K. Mohanty, and H. Hinrichsen, Fixed-Energy Sandpiles Belong Generically to Directed Percolation, *Phys. Rev. Lett.* **109**, 015702 (2012).
- [17] J. L. Cardy and R. L. Sugar, Directed percolation and Reggeon field theory, *J. Phys. A: Math. Gen.* **13**, L423 (1980).
- [18] S. Lübeck and P. C. Heger, Universal finite-size scaling behavior and universal dynamical scaling behavior of absorbing phase transitions with a conserved field, *Phys. Rev. E* **68**, 056102 (2003); Universal Scaling Behavior at the Upper Critical Dimension of Nonequilibrium Continuous Phase Transitions, *Phys. Rev. Lett.* **90**, 230601 (2003).
- [19] P. K. Mohanty and D. Dhar, Generic Sandpile Models Have Directed Percolation Exponents, *Phys. Rev. Lett.* **89**, 104303 (2002).
- [20] T. E. Harris, Contact process on a lattice, *Ann. Probab.* **2**, 969 (1974).
- [21] I. Jensen and R. Dickman, Nonequilibrium phase transitions in systems with infinitely many absorbing states, *Phys. Rev. E* **48**, 1710 (1993).
- [22] S. Kwon and J. M. Kim, Critical behavior for random initial conditions in the one-dimensional fixed-energy Manna sandpile model, *Phys. Rev. E* **94**, 012113 (2016).
- [23] S. Kwon and J. M. Kim, Effects of random initial conditions on the dynamical scaling behaviors of a fixed-energy Manna sandpile model in one dimension, *Phys. Rev. E* **91**, 012149 (2015).
- [24] S. Torquato and F. H. Stilling, Local density fluctuations, hyperuniformity, and order metrics, *Phys. Rev. E* **68**, 041113 (2003).
- [25] D. Hexner and D. Levine, Hyperuniformity of Critical Absorbing States, *Phys. Rev. Lett.* **114**, 110602 (2015).
- [26] S. B. Lee, Hyperuniformity and absorbing phase transition in continuous media with a conserved field, *J. Stat. Mech.* (2019) 053201.
- [27] S. B. Lee, Universality class of the conserved Manna model in one dimension, *Phys. Rev. E* **89**, 060101(R) (2014).
- [28] S. Kwon and J. M. Kim, Critical behavior of a fixed-energy Manna sandpile model for regular initial conditions in one dimension, *Phys. Rev. E* **92**, 062149 (2015).
- [29] S. B. Lee, Universality of continuous and discrete conserved Manna models in one dimension, *J. Stat. Mech.* (2017) 083204.
- [30] R. Dickman and S. D. da Cunha, Particle-density fluctuations and universality in the conserved stochastic sandpile, *Phys. Rev. E* **92**, 020104(R) (2015).
- [31] S. B. Lee, Comment on “Fixed-Energy Sandpiles Belong Generically to Directed Percolation”, *Phys. Rev. Lett.* **110**, 159601 (2013).
- [32] S. B. Lee, Critical behavior of absorbing phase transitions for models in the Manna class with natural initial states, *Phys. Rev. E* **89**, 062133 (2014).
- [33] P. Bak, C. Tang, and K. Wiesenfeld, Self-Organized Criticality: An Explanation of $1/f$ Noise, *Phys. Rev. Lett.* **59**, 381 (1987); Self-organized criticality, *Phys. Rev. A* **38**, 364 (1988).
- [34] S. S. Manna, Two-state model of self-organized criticality, *J. Phys. A: Math. Gen.* **24**, L363 (1991).
- [35] M. J. de Oliveira, Conserved lattice gas model with infinitely many absorbing states in one dimension, *Phys. Rev. E* **71**, 016112 (2005).
- [36] S. B. Lee and S. Lee, Absorbing phase transition in a conserved lattice gas model in one dimension, *Phys. Rev. E* **77**, 021113 (2008).